SPARC-EBD-11/001
April 28, 2011

Accurate, multi-purpose, real-time ROI and size measurement for e-beam diagnostic at SPARC experiment.

M. Quattromini and V. Surrenti†
*C.R.E. ENEA-Frascati, Via E. Fermi 45, 00044 Frascati (Rome) Italy**

In this note the problem of fast and accurate measurement of electron beam size for diagnostic purposes is addressed, with focus to emittance measurement via quadrupole scans and beam matching. An algorithm is devised that rapidly determines a region of interest where most of the signal is concentrated, not requiring acquisition and subtraction of background. The performances of the method are discussed in a variety of contexts relevant to a set of measures routinely performed during runs at SPARC[1] experiment. Although the algorithms are remarkably fast, little or no emphasis is devoted in this note to time performances, postoponing to a forthcoming note a thorough analysis of execution speed and a prospective real time implementation.

*Dedicated to the lovely memory of our mothers Fedora and Maria, who were happily among us when this work was commenced, and now are not anymore.

I. INTRODUCTION

In this note the problem of fast, accurate identification of the Region Of Interest ("ROI", hereafter) in the picture of the transverse configuration space of an electron beam impinging onto an imaging device is addressed. Many factors contribute to render the automation of such a task cumbersome, first of all the incumbence of a wide, spiky noise dotting the image, as is clearly visible, for example, in fig. (1). The presence of noise thwarts the accurate evaluation of statistical properties as centroid's average position and size, which are crucial for measurements of e.g. transverse emittance in quadrupole scans, energy or beam longitudinal tomography. Fast completion of the task is not as much a requirement unless short term stability is a concern, but remains nevertheless a desirable feature, not to mention the absence of bias inherent to automated execution with respect to procedures involving at any stage direct inspection by human operators. Moreover, even though the technique described here benefits from acquisition and subtraction of background - especially when a substantial dark current is present contributing a charge comparable to that of accelerated bunch - this is not strictly necessary, which may considerably improve time performances. The document layout is the following: in the next section the algorithm devoted to fast ROI identification is described. In the third section the effects of noise on spot's centroid and size assessment are investigated along with various approaches aiming at improving accuracy. Results against synthetic images are checked in the fourth section. Fifth section briefly examplifies the functioning of the algorithm for images acquired in other cases from the primary context of electron beams. Sixth and last section is devoted to final remarks and conclusions.

II. AUTOMATED ROI IDENTIFICATION PROCEDURE.

The algorithm adopted to identify the ROI is divided in two parts. The first is essentially a process of erosion, summarized by the pseudo-code snippet in Algorithm (1).

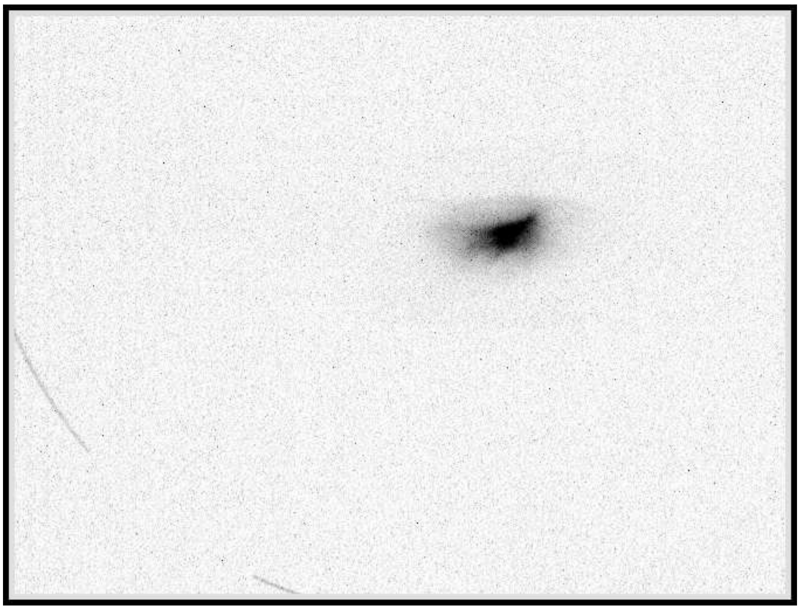

Figure 1: A typical e-beam spot acquired for q-scan emittance measurement. The image has been normalized and negated for clarity. The arc-like pattern on the left-bottom corner is an artifact of the target plate used for e-beam imaging.

Algorithm 1 FIRE (**F**ast **I**mage **R**OI **E**xtraction) 1$^{\mathrm{st}}$ part ($\rightarrow$image erosion).

1: **procedure** EROSION(*image*)
2: SMOOTH(image,r) ▷ Reduce "salt-pepper" noise by replacing each pixel with the median value in a pixel window of radius r. Optional. Strongly reccomended.
3: SETMINGRAYLEVEL(image,0) ▷ Offset subtraction: $\mathrm{l_{min}} \leftarrow 0$, see below. Optional for ROI tagging. Critical to improve accuracy on rms estimation (Algorithm (2).
4: $n_{\mathrm{t}} \leftarrow$Thresholding coarseness. ▷ Set the maximum number of steps taken to span the intensity range of the image. Not critical, $n_{\mathrm{t}} \gtrsim 10 - 20$.
5: $i \leftarrow 1$ ▷ Starting value.
6: **repeat**
7: $t \leftarrow \mathrm{l_{min}} + i \times \dfrac{\mathrm{l_{max}} - \mathrm{l_{min}}}{n_{\mathrm{t}}}$ ▷ Sets the threshold level.
8: BLACKTHRESHOLD(image,t) ▷ Set to zero all pixels with signal $< t$.
9: $\mathcal{A}^{(i)} \leftarrow$COUNTSURVIVORS(image) ▷ Count pixels with signal > 0.
10: $\mathcal{I}^{(i)} \leftarrow$COMPUTEINTEGRAL(image) ▷ Sum signal from survivors.
11: **if** $i > 1$ **then**
12: $r_{\mathcal{A}}^{(i)} \leftarrow \dfrac{\mathcal{A}^{(i-1)} - \mathcal{A}^{(i)}}{\mathcal{A}^{(i-1)}}$ ▷ Compute (relative) removed area.
13: $r_{\mathcal{I}}^{(i)} \leftarrow \dfrac{\mathcal{I}^{(i-1)} - \mathcal{I}^{(i)}}{\mathcal{I}^{(i-1)}}$ ▷ Compute (relative) removed signal.
14: **if** $r_{\mathcal{I}}^{(i)} > 0$ **then**
15: $\mathcal{R}^{(i)} \leftarrow \dfrac{r_{\mathcal{A}}^{(i)}}{r_{\mathcal{I}}^{(i)}}$ ▷ Compute trade-off ratio. between rejected area/signal
16: **if** $\mathcal{R}^{(i)} > \mathcal{R}^{(i-1)}$ **then** ▷ If $\mathcal{R}^{(i)}$ didn't peak yet...
17: $i \leftarrow i + 1$ ▷ ...Go for another iteration
18: **else** ▷ ... Else ...
19: $\mathrm{last_i} \leftarrow i - 1$ ▷ Take a step back ...
20: exitcondition $\leftarrow$ True ▷ ... Signal exit condition and ...
21: break ▷ ... Exit loop
22: **end if**
23: **end if**
24: **end if**
25: **until** $i < n_{\mathrm{t}} \vee$ exitcondition $\neq$True
26: **end procedure**

Some comments are in order to elucidate how the procedure works:

- The smoothing procedure mentioned at step (2) replaces each pixel with its neighbor closest in value. A neighbor is a structuring element defined by a radius, for example a square $(2r + 1) \times (2r + 1)$ pixels wide. A value of zero plays of course no effect. In the current analysis has been used a value $r = 2$. Note that the main effect of this operation is suppression of defective, isolated pixels on the camera's imaging device, (i.e. "dead" pixels always on or off).

- The main iteration (steps 6-25) consists of a **progressive black-thresholding**, that continues until the ratio $\mathcal{R}^{(i)}$ (step 15) between the relative removed area $r_{\mathcal{A}}^{(i)}$ (step 12) and the relative removed signal $r_{\mathcal{I}}^{(i)}$ (step 13) first peaks. $\mathcal{R}^{(i)}$ exhibits indeed a very clear maximum (see fig. 2). The idea behind this is that most of the signal is localized in a narrow region surrounded by a very wide though shallow background, dotted of spiky, isolated peaks, contributing altogether an overwhelming fraction of the total integral. A wide background, moreover, seriously affects the accurate reconstruction of signal' distribution first momenta (essentialy average position and r.m.s.) needed in a variety of cases, e.g. during emittance quadrupole scans.

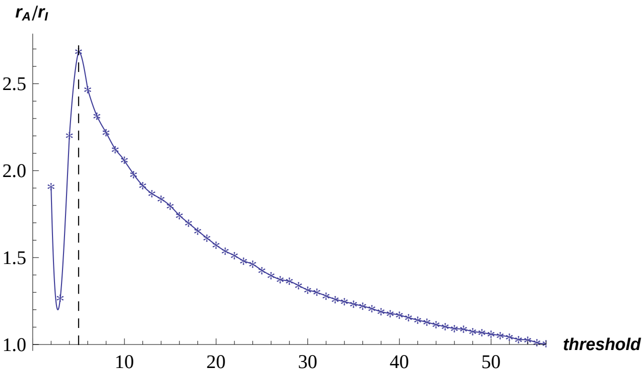

Figure 2: $\mathcal{R} = \dfrac{r_\mathcal{A}}{r_\mathcal{I}}$ vs threshold (step 15 in Algorithm 1) for the image in fig (1).

- Progressive black-thresholding image is expected to erode initially more *area* - that is, pixels hosting mainly background - than *signal* - to be understood here as the *bona fide* superposition of *real* signal *and* noise. This is the case indeed clearly visible in figure (3), where the surviving total area $t_\mathcal{A}$ and the total integral $t_\mathcal{I}$ (as fractions of the entire image quantities) are plotted vs the threshold level. It is worth remarking that although the very first step is usually the most effective at removing a large fraction of background pixels, it is by no means the best compromise between noise rejection and loss of signal. This is best substantiated in fig. (4), where is clear that maxima of both $r_\mathcal{A}^{(i)}$ and $r_\mathcal{I}^{(i)}$ occur at a lower threshold than the value that maximizes the *ratio* between them (the dashed vertical line). Usually one or more steps are required to achieve $\mathcal{R}$'s maximum, signalling a condition whereupon further thresholding implies a negative trend in relative signal-to-noise erosion.

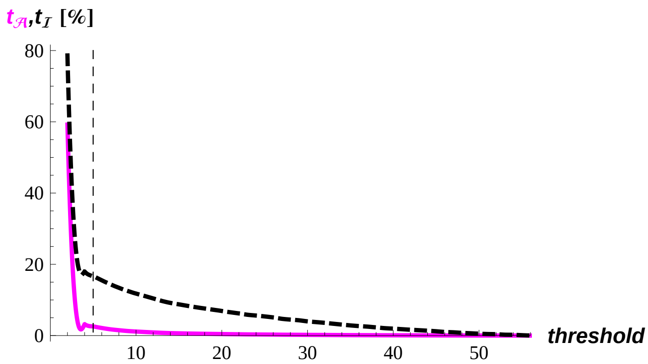

Figure 3: Relative total area ($t_\mathcal{A}$) and integral ($t_\mathcal{I}$) surviving a given black-threshold level for e-beam image in fig. (1). Total area decreases much faster than signal with increasing threshold levels. The vertical dashed line signals the position of maximum in fig. (2).

The effect of image erosion through progressive black-thresholding is illustrated in fig. (5). It is worth remarking that erosion (as of pseudo-code in Algorithm 1) does not really define any ROI. It may strongly restricts the image support - the set of pixels where the distribution is strictly positive - which by no means is warranted to form a connected domain embodying the signal. In order to introduce a rigorous, quantitative definition of ROI let

$$\begin{aligned} \mu &\equiv \frac{\mathcal{I}^{(1)}}{\mathcal{I}^{(0)}} \equiv \overline{w} \\ \widehat{\sigma} &\equiv \frac{\mathcal{I}^{(2)}}{\mathcal{I}^{(0)}} - \mu \cdot \mu^{\mathrm{T}} \end{aligned} \tag{1}$$

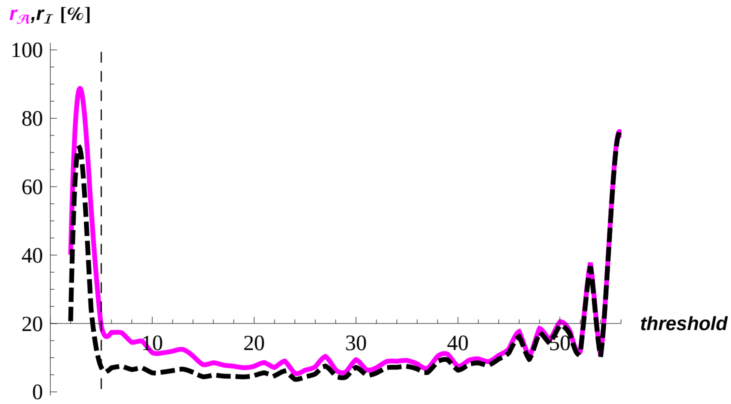

Figure 4: Relative removed total area ($r_{\mathcal{A}}$) and integral ($r_{\mathcal{I}}$) vs black-threshold level for e-beam image in fig. (1). Maxima occur at thresholds lower than level at which $r_{\mathcal{A}}/r_{\mathcal{I}}$ first peaks (dashed vertical line).

be the centroid's average position and covariance (that is r.m.s.) matrix at a given level in the thresholding process and

$$\begin{aligned} \mathcal{I}^{(0)} &\equiv \sum_{x,y} \mathcal{I}(w) \\ \mathcal{I}^{(1)} &\equiv \sum_{x,y} \mathcal{I}(w) \cdot w \qquad \text{with } w \equiv \begin{pmatrix} x \\ y \end{pmatrix} \\ \mathcal{I}^{(2)} &\equiv \sum_{x,y} \mathcal{I}(w) \cdot \left[w \cdot w^{\mathrm{T}} \right] \end{aligned} \tag{2}$$

the 0^{th}, 1^{st} and 2^{nd} order distribution's momenta of the intensity $\mathcal{I}(w)$ at pixel of coordinates $w \equiv (x, y)$. In terms of (2), a region of interest can be defined as the domain:

$$\mathcal{D}_n \equiv \left\{ w \ni (w - \overline{w})^{\mathrm{T}} \cdot \widehat{\sigma}^{-1} \cdot (w - \overline{w}) \leq n^2 \right\} \tag{3}$$

where

$$\widehat{\sigma} \equiv \frac{\mathcal{I}^{(2)}}{\mathcal{I}^{(0)}} - \frac{\mathcal{I}^{(1)} \cdot \mathcal{I}^{(1)\mathrm{T}}}{\left(\mathcal{I}^{(0)}\right)^2} \tag{4}$$

is the r.m.s. matrix and n^2 is a (positive) quantity. The equation (3) defines the interior of a family of ellipses, like those drawn over frames in fig. (5), corresponding to $n = 3$. The crossing lines reflect centroid's average position and orientation ot the ellipse itself. Note that the ellipse in the second frame is not missing, it is merely so large to include the whole image, while that in the last frame (the final step in thresholding procedure) defines a safeguard region completely embodying the seeked signal, almost unbiased by the long-range, *snow-like* noise

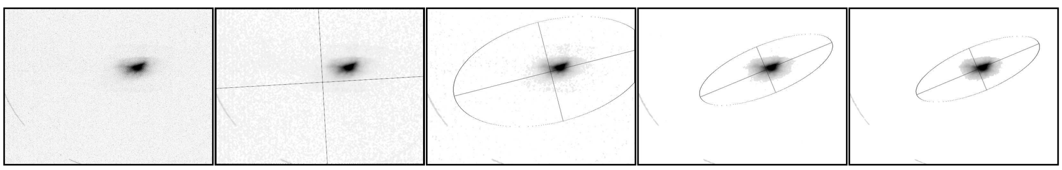

Figure 5: Effects of image erosion. The leftmost frame in the sequence is the same 8−bit image as in fig. (1), while the following snapshots corresponds to the same image after progressive black-thresholding with levels equal to $\mathtt{l} = 2, 3, 4, 5$. Thresholding was preceded by the preliminary noise reduction described in algorithm (1), step (2). Images have been normalized for clarity. Maximum level in the original was $\mathtt{l} = 56$.

affecting the original, yet still plagued by the arc-like artifacts mentioned above. Clearly some further refinement is in order to pinpoint a recipe entailing a sound estimation of distribution' r.m.s. size. A working, euristic prescription is sketched in the pseudocode below:

Algorithm 2 FIRE (**F**ast **I**mage **R**OI **E**xtraction) 2^{nd} part ($\rightarrow$ROI definition, masking).

---

procedure MASKING($\mathcal{I}$) $\triangleright$ $\mathcal{I}$ is the image resulting from thresholding procedure described in the 1^{st} part.

$\{\mathcal{I}_0, \mathcal{I}_1, \mathcal{I}_2\} \leftarrow$COMPUTEMOMENTA($\mathcal{I}$) $\triangleright$ Compute 0^{th}, 1^{st} and 2^{nd} order image momenta (eqs.(1,2)).

$\{\mu, \widehat{\sigma}\} \leftarrow$COMPUTESTAT($\mathcal{I}_0, \mathcal{I}_1, \mathcal{I}_2$) $\triangleright$ Compute distribution's centroid and r.m.s. size.

$\mathcal{M} \leftarrow$DEFINEROI($\mu, \widehat{\sigma}, n$) $\triangleright$ Define a *mask*, i.e. an image which is 1 inside the ellipse in eq. (3), 0 elsewhere. **This is the ROI.**

$\widetilde{\mathcal{I}} \leftarrow$APPLYROIMASK($\mathcal{I}, \mathcal{M}$) $\triangleright$ Apply mask $\mathcal{M}$ to $\mathcal{I}$.

$\left\{\widetilde{\mathcal{I}}_0, \widetilde{\mathcal{I}}_1, \widetilde{\mathcal{I}}_2\right\} \leftarrow$COMPUTEMOMENTA($\widetilde{\mathcal{I}}$) $\triangleright$ Compute 0^{th}, 1^{st} and 2^{nd} order *masked* image momenta (eqs.(1,2)).

$\left\{\widetilde{\mu}, \widetilde{\widehat{\sigma}}\right\} \leftarrow$COMPUTESTAT($\widetilde{\mathcal{I}}_0, \widetilde{\mathcal{I}}_1, \widetilde{\mathcal{I}}_2$) $\triangleright$ Compute *masked* distribution's centroid and r.m.s. size.

end procedure

In a nutshell, the 2^{nd} part of the algorithm can be summarized as follows:

- Define the ROI as the ellipse in last frame of fig. (5), corresponding to the final step in thresholding procedure described in the 1^{st} part, through eq. (3) for a suitable value of n ($n \gtrsim 3$ is a safe choice);
- define a *mask*, that is a *stencil* image with pixel content equal to 1 on the ROI, 0 elsewhere; apply the mask, that is multiply pixel-by-pixel the mask by the thresholded image emerging from erosion part of the algorithm; compute centroid's position and r.m.s. beam size from eqs. (1);
- define the *core* signal as the fraction of the image falling inside an embodying ellipse computed for a suitable value n (e.g. the same value used for the ROI).

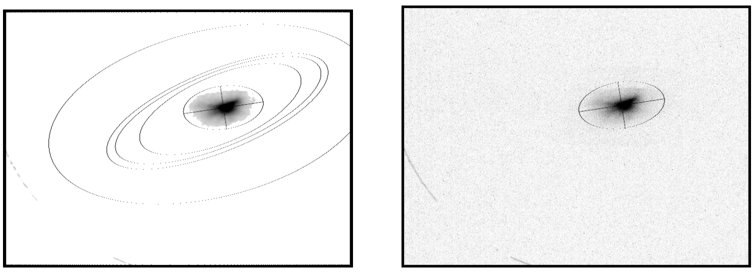

(a) (b)

Figure 6: Left (a): the result of procedure described in Algorithm (2). Right (b): The final ellipse drawn over the original, noisy image.

The result of such a procedure are illustrated in fig. (6a) for the same sequence as in fig. (5). In the left frame the family of ellipses defining the ROI at progressive black-thresholding levels are superimposed along with the (innermost) one embodying the core; in fig. (6b) this very last ellipse is drawn alone on the original, noisy snapshot. Another glimpse of the algorithm working

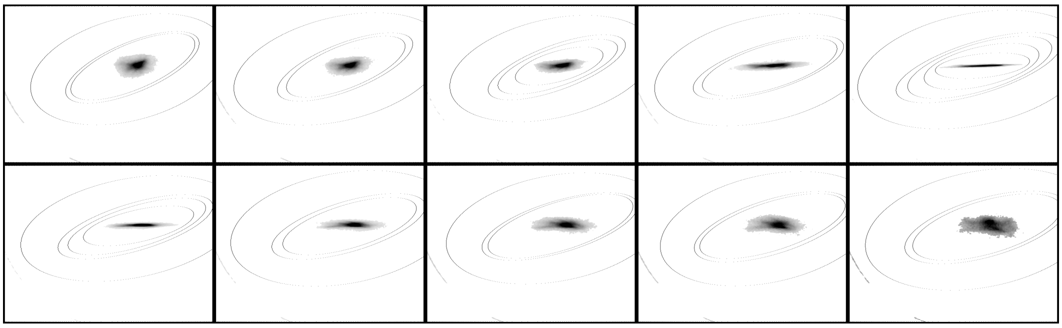

Figure 7: Result of ROI tagging for a sequence of ten images acquired during a 4-pole scan. Top-left frame corresponds to image in fig. (1). The drawn ellipses corresponds to a value $n = 3$ in (3) at different stages during algorithm's iterations.

can be seen in fig. (7), where the frames in the sequence corresponds to snapshots acquired during a quadrupole scan, the left-top frame being the same as fig. (6a). Visual inspection of the sequences of shrinking ellipses in each snapshot clearly suggests that ROIs at pristine stages of the procedure are largely determined by the background, including the arc-like artifacts visible in left-bottom corner (which outline the boundaries of the plate the electron beam impinges upon). In fact, outermost ellipses look much the same in the ten frames, differentiating one from the other at final steps only, where ROIs look finally as a sound guesses of the signal position, size and orientation.

Note that for a 2D gaussian profile (like that described by eq. (26) below), which is usually a reasonable assumption, it can be easily proven that the domain (3) includes a fraction $\left[1 - \exp\left(-\frac{n^2}{2}\right)\right]$ of the total signal.

In the following section the estimation accuracy of statistical properties of signal inside ROI will be discussed, with much emphasis devoted to the problem of residual noise surviving the cut, treatment of various diseases arising e.g. from digital quantization, and a few idiosyncrasies related to specific image formats.

III. EFFECTS OF NOISE ON R.M.S. VALUES. RMS MATRIX CORRECTION.

Consider the ellipse in fig. 8, delimiting the ROI derived in the previous section, which for sake of simplicity has been assumed to be centrated at origin. Assuming that the signal is entirely localized in this region, one can safely discard any information falling outside, greatly reducing the effect of noise compromising the accuracy of r.m.s. size's measurement. In this section an analytical procedure is devised to assess the noise level and derive a formula to compensate its effect on spot size. In Appendices A and B can be found some customary algebra exploiting the transformation properties of fundamental objects (vectors, tensors) in the 2D-plane, which turns handy in order to reduce the amount of calculations in the following analysis. Let $\mathcal{F}(x, y)$ be the scalar function associated to the signal over the ROI. Accordingy with (2), the $0^{\text{th}}, 1^{\text{st}}$ and 2^{nd} momenta associated can be written in compact form as

$$\begin{aligned}
\mathcal{I}_{\mathcal{D}}^{(0)}(\mathcal{F}) &\equiv \int_{\mathcal{D}} d^2w\, \mathcal{F}(w) \\
\mathcal{I}_{\mathcal{D}}^{(1)}(\mathcal{F}) &\equiv \int_{\mathcal{D}} d^2w\, \mathcal{F}(w)\, w \\
\mathcal{I}_{\mathcal{D}}^{(2)}(\mathcal{F}) &\equiv \int_{\mathcal{D}} d^2w\, \mathcal{F}(w) \left[w \cdot w^{\mathrm{T}}\right]
\end{aligned} \tag{5}$$

where

$$w \equiv \begin{pmatrix} x \\ y \end{pmatrix} \qquad d^2w \equiv dx \cdot dy$$

Finally, let $\mathcal{D}$ is the domain associated to the ROI:

$$\mathcal{D} \equiv \left\{ w \ni \left[(w-d)^{\mathrm{T}} \cdot \widehat{\mathcal{S}}^{-1} \cdot (w-d) \right] \leq n^2 \right\} \tag{6}$$

where

$$d \equiv \begin{pmatrix} d_x \\ \\ d_y \end{pmatrix} \tag{7}$$

(see fig. (8)) and $\mathcal{S}$ is the matrix associated to the ROI (that is the r.m.s. matrix of the original image optimally black-thresholded). Let ω denote the generic vector in the frame (ξ, η):

$$\omega \equiv \begin{pmatrix} \xi \\ \\ \eta \end{pmatrix} \tag{8}$$

Although an accurate disentanglement of the signal is an awkward task, especially on spot's boundaries where it is inherently impossible to distinguish from noise, as long as the emphasis is on statistical properties, one can always assume that the observed spot is described by a function $\mathcal{F}$ resulting from the superposition of a *genuine* signal - which will be denoted by $f(w)$ - and a noise $\mathcal{N}(w)$ spread all over the image:

$$\mathcal{F}(w) = f(w) + \mathcal{N}(w) \tag{9}$$

Consistently with definitions (2,5) and (9) it follows then

$$\begin{aligned} \mathcal{I}_{\mathcal{D}}^{(0)}[\mathcal{F}] &= \mathcal{I}_{\mathcal{D}}^{(0)}[f] + \mathcal{I}_{\mathcal{D}}^{(0)}[\mathcal{N}] \\ \mathcal{I}_{\mathcal{D}}^{(1)}[\mathcal{F}] &= \mathcal{I}_{\mathcal{D}}^{(1)}[f] + \mathcal{I}_{\mathcal{D}}^{(1)}[\mathcal{N}] \\ \mathcal{I}_{\mathcal{D}}^{(2)}[\mathcal{F}] &= \mathcal{I}_{\mathcal{D}}^{(2)}[f] + \mathcal{I}_{\mathcal{D}}^{(2)}[\mathcal{N}] \end{aligned} \tag{10}$$

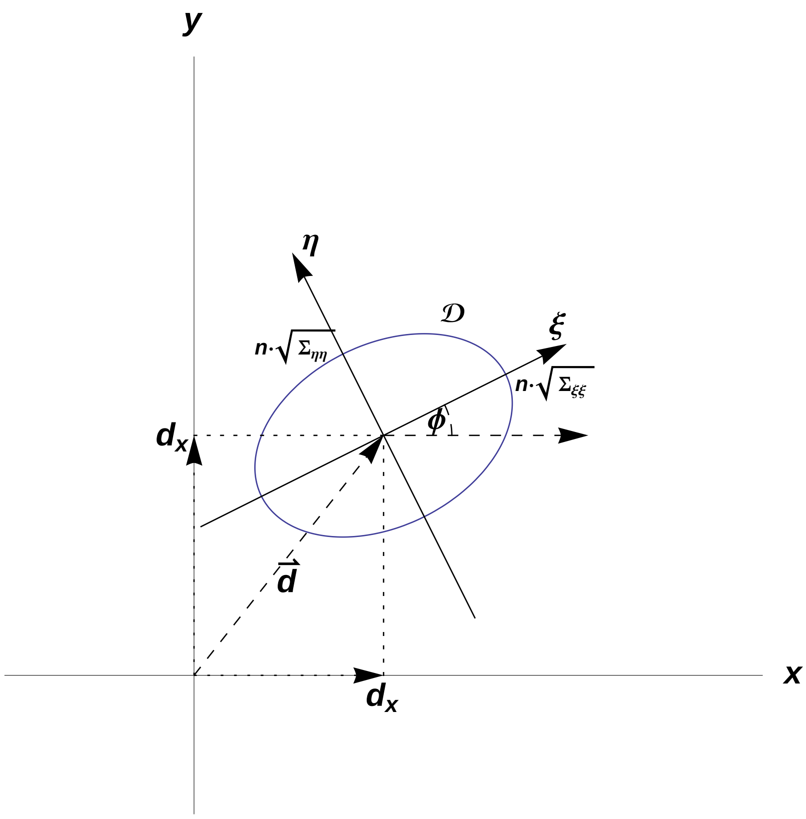

Figure 8

Formulæ (10) come handy whenever background images are available for which one can *bona fide* assume the content to be the same as the noise $\mathcal{N}(w)$ of the images to be analyzed. This is the case, for example, of dark current in electron beams and is to be understood - of course - only in a statistical sense for one aims only at an independent evaluation of noise momenta $\mathcal{I}_{\mathcal{D}}^{(k)}[\mathcal{N}]$. Alternatively, the further assumption (whenever plausible) that the function $\mathcal{N}(w)$ be *homogeneous*:

$$\mathcal{N}(w) = \kappa \Longrightarrow \mathcal{F}(w) = f(w) + \kappa \tag{11}$$

allows the derivation of an analytical correction factor relatively immune from artifacts due e.g. to limited bitdepth in ADC conversion at DAQ stage, or the format utilized for image storage. The two cases will be now treated separately, with some emphasis devoted to error assessment.

A. Homogeneous noise.

Whenever (11) applies, formulæ (10) read

$$\begin{aligned}
\mathcal{I}_{\mathcal{D}}^{(0)}[\mathcal{F}] &= \mathcal{I}_{\mathcal{D}}^{(0)}[f] + \kappa\mathcal{J}_{\mathcal{D}}^{(0)} \\
\mathcal{I}_{\mathcal{D}}^{(1)}[\mathcal{F}] &= \mathcal{I}_{\mathcal{D}}^{(1)}[f] + \kappa\mathcal{J}_{\mathcal{D}}^{(1)} \\
\mathcal{I}_{\mathcal{D}}^{(2)}[\mathcal{F}] &= \mathcal{I}_{\mathcal{D}}^{(2)}[f] + \kappa\mathcal{J}_{\mathcal{D}}^{(2)}
\end{aligned} \tag{12}$$

where

$$\mathcal{J}_{\mathcal{D}}^{(0)} = \int_{\mathcal{D}} d^2w$$

is nothing but the area $\mathcal{A}_{\mathcal{D}}$ of domain $\mathcal{D}$ (that is $\mathcal{J}_{\mathcal{D}}^{(0)} = \mathcal{A}_{\mathcal{D}}$) while

$$\begin{aligned}
\mathcal{J}_{\mathcal{D}}^{(1)} &\equiv \int_{\mathcal{D}} d^2w\, w \\
\mathcal{J}_{\mathcal{D}}^{(2)} &\equiv \textstyle\int_{\mathcal{D}} d^2w\, \left(w \cdot w^{\mathrm{T}}\right)
\end{aligned}$$

are the 1$^{\mathrm{st}}$ and 2$^{\mathrm{nd}}$ momenta of the constant function $f(w) = 1$. Since $\mathcal{D}$ is the ellipse defined by any of eqs. (6), (B5) and (B6), it is easily proven that (see (B7))

$$\mathcal{J}_{\mathcal{D}}^{(0)} \equiv \mathcal{A}_{\mathcal{D}} = \pi n^2 \sqrt{\det \widehat{\mathcal{S}}} \tag{13}$$

while $\mathcal{J}_{\mathcal{D}}^{(1)}$ is obviously $\mathcal{A}_{\mathcal{D}}$ times the center of the ROI $\mu_{\mathcal{D}} \equiv d$:

$$\mathcal{J}_{\mathcal{D}}^{(1)} = \mathcal{A}_{\mathcal{D}} d \tag{14}$$

The calculation of $\mathcal{J}_{\mathcal{D}}^{(2)}$ is worked out in Appendix B (eqs. (B13-B15)) and turns to be

$$\mathcal{J}_{\mathcal{D}}^{(2)} = \mathcal{A}_{\mathcal{D}} \left[\frac{n^2}{4}\widehat{\mathcal{S}} + d \cdot d^{\mathrm{T}}\right] \tag{15}$$

It is worth noting, *en passant,* that for $f = 0$, formulæ(1),(15) yield

$$\widehat{\sigma}_{\mathcal{D}}(\mathcal{F} = \kappa) \equiv \frac{\mathcal{I}_{\mathcal{D}}^{(2)}[\mathcal{F}]}{\mathcal{I}_{\mathcal{D}}^{(0)}[\mathcal{F}]} - \frac{\mathcal{I}_{\mathcal{D}}^{(1)}[\mathcal{F}] \cdot \mathcal{I}_{\mathcal{D}}^{(1)\mathrm{T}}[\mathcal{F}]}{\left(\mathcal{I}_{\mathcal{D}}^{(0)}[\mathcal{F}]\right)^2} = \frac{\mathcal{J}_{\mathcal{D}}^{(2)}}{\mathcal{J}_{\mathcal{D}}^{(0)}} - \frac{\mathcal{J}_{\mathcal{D}}^{(1)} \cdot \mathcal{J}_{\mathcal{D}}^{(1)\mathrm{T}}}{\left(\mathcal{J}_{\mathcal{D}}^{(0)}\right)^2} = \frac{n^2}{4}\widehat{\mathcal{S}}$$

which generalize, the well known result that for an uniform distribution over a circle of radius ρ the components of the r.m.s. matrix are given by $\sigma_{xx} = \sigma_{yy} = \rho^2/4$.

The *corrected* r.m.s. tensor $\widehat{\sigma}_{\mathcal{D}}(f)$ can be cast in terms of the *rough estimate* $\widehat{\sigma}_{\mathcal{D}}(F)$ with some manipulations (cfr (1)):

$$\begin{aligned}\widehat{\sigma}_{\mathcal{D}}(f) &\equiv \frac{\mathcal{I}^{(2)}_{\mathcal{D}}[f]}{\mathcal{I}^{(0)}_{\mathcal{D}}[f]} - \mu_{\mathcal{D}}[f]\cdot\mu_{\mathcal{D}}[f]^{\mathrm{T}} \\ \mu_{\mathcal{D}}[f] &\equiv \frac{\mathcal{I}^{(1)}_{\mathcal{D}}[f]}{\mathcal{I}^{(0)}_{\mathcal{D}}[f]}\end{aligned}$$

where

$$\mu_{\mathcal{D}}[f] = \frac{\mathcal{I}^{(1)}_{\mathcal{D}}[\mathcal{F}] - \kappa\mathcal{J}^{(1)}_{\mathcal{D}}}{\mathcal{I}^{(0)}_{\mathcal{D}}[\mathcal{F}]}\frac{\mathcal{I}^{(0)}_{\mathcal{D}}[\mathcal{F}]}{\mathcal{I}^{(0)}_{\mathcal{D}}[\mathcal{F}] - \kappa\mathcal{A}_{\mathcal{D}}} = \left[\mu_{\mathcal{D}}[\mathcal{F}] - \kappa\frac{\mathcal{A}_{\mathcal{D}}}{\mathcal{I}^{(0)}_{\mathcal{D}}[\mathcal{F}]}d\right]\left[\frac{1}{1-\kappa\mathcal{A}_{\mathcal{D}}/\mathcal{I}^{(0)}_{\mathcal{D}}[\mathcal{F}]}\right]$$

Denoting by

$$\langle\mathcal{F}\rangle_{\mathcal{D}} \equiv \frac{\mathcal{I}^{(0)}_{\mathcal{D}}[\mathcal{F}]}{\mathcal{A}_{\mathcal{D}}}$$

the average of F over the domain $\mathcal{D}$, it follows

$$\mu_{\mathcal{D}}[f] = \frac{\langle\mathcal{F}\rangle_{\mathcal{D}}}{\langle\mathcal{F}\rangle_{\mathcal{D}} - \kappa}\left[\mu_{\mathcal{D}}[\mathcal{F}] - \frac{\kappa d}{\langle\mathcal{F}\rangle_{\mathcal{D}}}\right]$$

(note that$\langle\mathcal{F}\rangle_{\mathcal{D}} - \kappa = \langle f\rangle_{\mathcal{D}}$). By following the same approach it is possible to derive a similar formula for the corrected covariance matrix:

$$\begin{aligned}\widehat{\sigma}_{\mathcal{D}}[f] &= \frac{\mathcal{I}^{(0)}_{\mathcal{D}}[\mathcal{F}]}{\mathcal{I}^{(0)}_{\mathcal{D}}[\mathcal{F}] - \kappa\mathcal{A}_{\mathcal{D}}}\frac{\mathcal{I}^{(2)}_{\mathcal{D}}[\mathcal{F}] - \kappa\mathcal{J}^{(2)}_{\mathcal{D}}}{\mathcal{I}^{(0)}_{\mathcal{D}}[\mathcal{F}]} - \mu_{\mathcal{D}}[f]\cdot\mu_{\mathcal{D}}[f]^{\mathrm{T}} \\ &= \frac{\langle\mathcal{F}\rangle_{\mathcal{D}}}{\langle\mathcal{F}\rangle_{\mathcal{D}} - \kappa}\left[\widehat{\sigma}_{\mathcal{D}}[\mathcal{F}] + \mu_{\mathcal{D}}[\mathcal{F}]\cdot\mu^{\mathrm{T}}_{\mathcal{D}}[\mathcal{F}] - \frac{\kappa}{\langle F\rangle_{\mathcal{D}}}\left(\frac{n^2}{4}\widehat{\mathcal{S}} + d\cdot d^{\mathrm{T}}\right)\right. \\ &\left.- \frac{\langle\mathcal{F}\rangle_{\mathcal{D}}}{\langle\mathcal{F}\rangle_{\mathcal{D}} - \kappa}\left(\mu_{\mathcal{D}}[\mathcal{F}] - \frac{\kappa d}{\langle\mathcal{F}\rangle_{\mathcal{D}}}\right)\cdot\left(\mu_{\mathcal{D}}[\mathcal{F}] - \frac{\kappa d}{\langle\mathcal{F}\rangle_{\mathcal{D}}}\right)^{\mathrm{T}}\right] \\ &= \frac{\langle\mathcal{F}\rangle_{\mathcal{D}}}{\langle\mathcal{F}\rangle_{\mathcal{D}} - \kappa}\left[\widehat{\sigma}_{\mathcal{D}}[\mathcal{F}] - \frac{\kappa}{\langle\mathcal{F}\rangle_{\mathcal{D}} - \kappa}\left(\mu_{\mathcal{D}}[\mathcal{F}]\cdot\mu^{\mathrm{T}}_{\mathcal{D}}[\mathcal{F}] + d\cdot d^{\mathrm{T}}\right) - \frac{\kappa n^2}{4\langle\mathcal{F}\rangle_{\mathcal{D}}}\widehat{\mathcal{S}}\right. \\ &\left.+ \frac{\kappa}{\langle\mathcal{F}\rangle_{\mathcal{D}} - \kappa}\left(d\cdot\mu^{\mathrm{T}}_{\mathcal{D}}[\mathcal{F}] + \mu_{\mathcal{D}}[\mathcal{F}]\cdot d^{\mathrm{T}}\right)\right] \\ &= \frac{\langle\mathcal{F}\rangle_{\mathcal{D}}}{\langle\mathcal{F}\rangle_{\mathcal{D}} - \kappa}\left\{\widehat{\sigma}_{\mathcal{D}}[\mathcal{F}] - \kappa\left[\frac{(d-\mu_{\mathcal{D}}[\mathcal{F}])\cdot(d-\mu_{\mathcal{D}}[\mathcal{F}])^{\mathrm{T}}}{\langle\mathcal{F}\rangle_{\mathcal{D}} - \kappa} - \frac{n^2\widehat{\mathcal{S}}}{4\langle\mathcal{F}\rangle_{\mathcal{D}}}\right]\right\}\end{aligned} \tag{16}$$

Note that derivation of eq. (16) is strictly functional only to error assessment analyzed below. From a progammer's point of view, it is much simpler use of eqs. (10) or - in the case that (11) applies - eqs. (12) In eqs. (16),(20) the only unknown parameter is κ, the average noise level underneath the signal. Assuming (see fig. (9)) that the signal is confined completelly inside the ROI (the domain $\mathcal{D} \equiv \mathcal{D}\left(\widehat{\mathcal{S}}, n^2\right)$ defined by eqs. (6) or (B4) as a combination of a r.m.s. matrix $\widehat{\mathcal{S}}$ and a positive number n^2, see formula (3)), a possible strategy is to define κ as the image average level in the area enclosed between the ROI and the boundary of a domain $\mathcal{D}\left(\widehat{\mathcal{S}}, N^2\right)$ defined by eq. (3) with a slightly larger value of positive parameter $N^2 > n^2$:

$$\kappa \approx \frac{\mathcal{I}^{(0)}_{\mathcal{D}\left(\widehat{\mathcal{S}},N^2\right)}[\mathcal{F}] - \mathcal{I}^{(0)}_{\mathcal{D}\left(\widehat{\mathcal{S}},n^2\right)}[\mathcal{F}]}{\mathcal{A}_{\mathcal{D}\left(\widehat{\mathcal{S}},N^2\right)} - \mathcal{A}_{\mathcal{D}\left(\widehat{\mathcal{S}},n^2\right)}} = \frac{1}{\pi\sqrt{\det\widehat{\mathcal{S}}}}\frac{\mathcal{I}^{(0)}_{\mathcal{D}\left(\widehat{\mathcal{S}},N^2\right)}[\mathcal{F}] - \mathcal{I}^{(0)}_{\mathcal{D}\left(\widehat{\mathcal{S}},n^2\right)}[\mathcal{F}]}{N^2 - n^2} \tag{17}$$

Formula (17) can be recast in the more suggestive fashion:

$$\kappa \approx \frac{1}{\pi\sqrt{\det\widehat{\mathcal{S}}}} \left.\frac{\partial\mathcal{I}^{(0)}_{\mathcal{D}(\widehat{\mathcal{S}},\nu)}[\mathcal{F}]}{\partial\nu}\right|_{\nu=n^2} \tag{18}$$

implying that

$$\mathcal{I}^{(0)}_{\mathcal{D}\left(\widehat{\mathcal{S}},N^2\right)}[\mathcal{F}] \approx \mathcal{I}^{(0)}_{\mathcal{D}\left(\widehat{\mathcal{S}},n^2\right)}[\mathcal{F}] + \kappa\pi\sqrt{\det\widehat{\mathcal{S}}}\left(N^2-n^2\right) \tag{19}$$

Formula (19) express nothing but the obvious fact that as soon n^2 is large enough for ROI to include the whole signal *and* noise is homogeneous outside, 1^{st} momentum grows linearly with the area of the ellipse $\left(\propto N^2\right)$. Such an expected behaviour provides a tool to *fit* values of κ, $\mathcal{I}^{(0)}_{\mathcal{D}\left(\widehat{\mathcal{S}},n^2\right)}$ and (optionally) n.

Observe now that

$$\mu_{\mathcal{D}}[\mathcal{F}] \approx d \qquad \Longrightarrow \qquad \widehat{\sigma}_{\mathcal{D}}[f] \approx \frac{\langle\mathcal{F}\rangle_{\mathcal{D}}}{\langle\mathcal{F}\rangle_{\mathcal{D}}-\kappa}\widehat{\sigma}_{\mathcal{D}}[\mathcal{F}] - \frac{\kappa}{\langle\mathcal{F}\rangle_{\mathcal{D}}-\kappa}\frac{n^2}{4}\widehat{\mathcal{S}} \tag{20}$$

which can be cast in the equivalent form

$$\widehat{\sigma}_{\mathcal{D}}[\mathcal{F}] = \frac{\langle\mathcal{F}\rangle_{\mathcal{D}}-\kappa}{\langle\mathcal{F}\rangle_{\mathcal{D}}}\widehat{\sigma}_{\mathcal{D}}[f] + \frac{\kappa}{\langle\mathcal{F}\rangle_{\mathcal{D}}}\frac{n^2}{4}\widehat{\mathcal{S}} \tag{21}$$

expressing the obvious result that if the barycentre ($\mu_{\mathcal{D}}[\mathcal{F}]$) of $\mathcal{F}$ does not differ substantially from the center (d) of the ROI, then $\widehat{\sigma}_{\mathcal{D}}[\mathcal{F}]$ can be expressed as the mean of the r.m.s. matrix of the signal $\widehat{\sigma}_{\mathcal{D}}[f]$ and the r.m.s. matrix of the noise $\frac{n^2}{4}\widehat{\mathcal{S}}$, weighted by the respective average values over $\mathcal{D}$. Formula (21) turns to be useful for a sound estimation of the error on $\widehat{\sigma}_{\mathcal{D}}[f]$ as a function of the other quantities involved. To this purpose, assuming for a moment the effects of signal quantization to be negligible with respect to statistical error on κ , estimated on the finite sample of pixels falling in between $\mathcal{D}\left(\widehat{\mathcal{S}},n^2\right)$ and $\mathcal{D}\left(\widehat{\mathcal{S}},N^2\right)$, i.e. that in eq. (21) only $\widehat{\sigma}_{\mathcal{D}}[f]$ and κ are affected by uncertainties, it follows by differentiation that

$$0 \approx \frac{1}{\langle\mathcal{F}\rangle_{\mathcal{D}}}\left\{\left[\widehat{\sigma}_{\mathcal{D}}[f] + \frac{\kappa}{\langle\mathcal{F}\rangle_{\mathcal{D}}}\frac{n^2}{4}\widehat{\mathcal{S}}\right]\delta\kappa - \kappa\cdot\delta\widehat{\sigma}_{\mathcal{D}}[f]\right\}$$

that is

$$\delta\widehat{\sigma}_{\mathcal{D}}[f] \approx \left(\widehat{\sigma}_{\mathcal{D}}[f] + \kappa\frac{n^2}{4\langle\mathcal{F}\rangle_{\mathcal{D}}}\widehat{\mathcal{S}}\right)\frac{\delta\kappa}{\kappa} \tag{22}$$

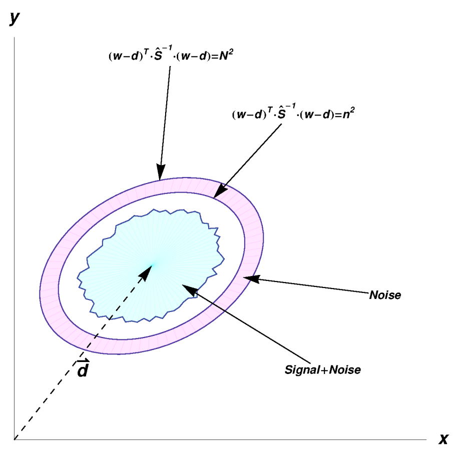

Figure 9

Formula (22) can be exploited to derive an expression of the relative error on $\widehat{\sigma}_{\mathcal{D}}[f]$ (note in fact that $\widehat{\sigma}_{\mathcal{D}}[f]$ is a matrix and the concept definition needs some care):

$$\frac{\delta\widehat{\sigma}_{\mathcal{D}}[f]}{\widehat{\sigma}_{\mathcal{D}}[f]} \equiv \widehat{\sigma}_{\mathcal{D}}^{-1}[f]\cdot\delta\widehat{\sigma}_{\mathcal{D}}[f] \approx \left[1+n^2\frac{\kappa}{4}\frac{\widehat{\sigma}_{\mathcal{D}}^{-1}[f]\cdot\widehat{\mathcal{S}}}{\langle\mathcal{F}\rangle_{\mathcal{D}}}\right]\frac{\delta\kappa}{\kappa} \tag{23}$$

showing that - roughly speaking - error propagation from κ to $\widehat{\sigma}_{\mathcal{D}}[f]$ is dominated by large values of n. Note also that factor $\kappa/\langle\mathcal{F}\rangle_{\mathcal{D}}$ although upper bounded to 1, gets more unfavourable for large n.

B. Inhomogeneous noise.

Let us devise now an analytical expression for the r.m.s. matrix in the case of an inhomogeneous noise. According to (1) and (12) corrected r.m.s. matrix $\widehat{\sigma}_{\mathcal{D}}(f)$ reads

$$\widehat{\sigma}_{\mathcal{D}}(f) \equiv \frac{\mathcal{I}_{\mathcal{D}}{}^{(2)}(\mathcal{F})-\mathcal{I}_{\mathcal{D}}{}^{(2)}(\mathcal{N})}{\mathcal{I}_{\mathcal{D}}{}^{(0)}(\mathcal{F})-\mathcal{I}_{\mathcal{D}}{}^{(0)}(\mathcal{N})} - \frac{\left[\mathcal{I}_{\mathcal{D}}{}^{(1)}(\mathcal{F})-\mathcal{I}_{\mathcal{D}}{}^{(1)}(\mathcal{N})\right]\cdot\left[\mathcal{I}_{\mathcal{D}}{}^{(1)}(\mathcal{F})-\mathcal{I}_{\mathcal{D}}{}^{(1)}(\mathcal{N})\right]^{\mathrm{T}}}{\left[\mathcal{I}_{\mathcal{D}}{}^{(0)}(\mathcal{F})-\mathcal{I}_{\mathcal{D}}{}^{(0)}(\mathcal{N})\right]^2}$$

Let us cast now $\mathcal{I}_{\mathcal{D}}^{(0)}(\mathcal{N})$ as follows

$$\mathcal{I}_{\mathcal{D}}^{(0)}(\mathcal{N}) = \frac{\mathcal{I}_{\mathcal{D}}^{(0)}(\mathcal{N})}{\mathcal{A}_{\mathcal{D}}}\frac{\mathcal{A}_{\mathcal{D}}}{\mathcal{I}_{\mathcal{D}}^{(0)}(\mathcal{F})}\mathcal{I}_{\mathcal{D}}^{(0)}(\mathcal{F}) = \frac{\langle\mathcal{N}\rangle_{\mathcal{D}}}{\langle\mathcal{F}\rangle_{\mathcal{D}}}\mathcal{I}_{\mathcal{D}}^{(0)}(\mathcal{F})$$

and assume that

$$\mu_{\mathcal{D}}[\mathcal{N}] \approx \mu_{\mathcal{D}}[\mathcal{F}] \quad \Longleftrightarrow \quad \frac{\mathcal{I}_{\mathcal{D}}^{(1)}(\mathcal{N})}{\mathcal{I}_{\mathcal{D}}^{(0)}(\mathcal{N})} \approx \frac{\mathcal{I}_{\mathcal{D}}^{(1)}(\mathcal{F})}{\mathcal{I}_{\mathcal{D}}^{(0)}(\mathcal{F})}$$

$$\Downarrow$$

$$\mathcal{I}_{\mathcal{D}}{}^{(1)}(\mathcal{N}) \approx \frac{\mathcal{I}_{\mathcal{D}}^{(0)}(\mathcal{N})}{\mathcal{I}_{\mathcal{D}}^{(0)}(\mathcal{F})}\mathcal{I}_{\mathcal{D}}^{(1)}(\mathcal{F}) = \frac{\langle\mathcal{N}\rangle_{\mathcal{D}}}{\langle\mathcal{F}\rangle_{\mathcal{D}}}\mathcal{I}_{\mathcal{D}}^{(1)}(\mathcal{F})$$

Thus

$$\begin{aligned}
\widehat{\sigma}_{\mathcal{D}}(f) &\approx \left(1-\frac{\langle\mathcal{N}\rangle_{\mathcal{D}}}{\langle\mathcal{F}\rangle_{\mathcal{D}}}\right)^{-1}\frac{\mathcal{I}_{\mathcal{D}}^{(2)}(\mathcal{F})-\mathcal{I}_{\mathcal{D}}^{(2)}(\mathcal{N})}{\mathcal{I}_{\mathcal{D}}^{(0)}(\mathcal{F})} - \frac{\mathcal{I}_{\mathcal{D}}^{(1)}(\mathcal{F})\cdot\mathcal{I}_{\mathcal{D}}^{(1)\mathrm{T}}(\mathcal{F})}{\left[\mathcal{I}_{\mathcal{D}}^{(0)}(\mathcal{F})\right]^2} \\
&= \left(1-\frac{\langle\mathcal{N}\rangle_{\mathcal{D}}}{\langle\mathcal{F}\rangle_{\mathcal{D}}}\right)^{-1}\left[\frac{\mathcal{I}_{\mathcal{D}}^{(2)}(\mathcal{F})-\mathcal{I}_{\mathcal{D}}^{(2)}(\mathcal{N})}{\mathcal{I}_{\mathcal{D}}^{(0)}(\mathcal{F})} - \left(1-\frac{\langle\mathcal{N}\rangle_{\mathcal{D}}}{\langle\mathcal{F}\rangle_{\mathcal{D}}}\right)\frac{\mathcal{I}_{\mathcal{D}}^{(1)}(\mathcal{F})\cdot\mathcal{I}_{\mathcal{D}}^{(1)\mathrm{T}}(\mathcal{F})}{\left[\mathcal{I}_{\mathcal{D}}^{(0)}(\mathcal{F})\right]^2}\right] \\
&= \left(1-\frac{\langle\mathcal{N}\rangle_{\mathcal{D}}}{\langle\mathcal{F}\rangle_{\mathcal{D}}}\right)^{-1}\left\{\overbrace{\left[\frac{\mathcal{I}_{\mathcal{D}}^{(2)}(\mathcal{F})}{\mathcal{I}_{\mathcal{D}}^{(0)}(\mathcal{F})} - \frac{\mathcal{I}_{\mathcal{D}}^{(1)}(\mathcal{F})\cdot\mathcal{I}_{\mathcal{D}}^{(1)\mathrm{T}}(\mathcal{F})}{\left[\mathcal{I}_{\mathcal{D}}^{(0)}(\mathcal{F})\right]^2}\right]}^{\widehat{\sigma}_{\mathcal{D}}(\mathcal{F})} - \frac{\mathcal{I}_{\mathcal{D}}^{(2)}(\mathcal{N})}{\mathcal{I}_{\mathcal{D}}^{(0)}(\mathcal{F})} + \frac{\langle\mathcal{N}\rangle_{\mathcal{D}}}{\langle\mathcal{F}\rangle_{\mathcal{D}}}\frac{\mathcal{I}_{\mathcal{D}}^{(1)}(\mathcal{F})\cdot\mathcal{I}_{\mathcal{D}}^{(1)\mathrm{T}}(\mathcal{F})}{\left[\mathcal{I}_{\mathcal{D}}^{(0)}(\mathcal{F})\right]^2}\right\} \\
&= \left(1-\frac{\langle\mathcal{N}\rangle_{\mathcal{D}}}{\langle\mathcal{F}\rangle_{\mathcal{D}}}\right)^{-1}\left\{\widehat{\sigma}_{\mathcal{D}}(\mathcal{F}) - \left[\frac{\mathcal{I}_{\mathcal{D}}^{(2)}(\mathcal{N})}{\mathcal{I}_{\mathcal{D}}^{(0)}(\mathcal{F})} - \frac{\langle\mathcal{N}\rangle_{\mathcal{D}}}{\langle\mathcal{F}\rangle_{\mathcal{D}}}\frac{\mathcal{I}_{\mathcal{D}}^{(1)}(\mathcal{F})\cdot\mathcal{I}_{\mathcal{D}}^{(1)\mathrm{T}}(\mathcal{F})}{\left[\mathcal{I}_{\mathcal{D}}^{(0)}(\mathcal{F})\right]^2}\right]\right\}
\end{aligned} \tag{24}$$

Let us cast now $\mathcal{I}^{(2)}(\mathcal{N})$ in the following form

$$\mathcal{I}^{(2)}_{\mathcal{D}}(\mathcal{N}) = \frac{\langle\mathcal{N}\rangle_{\mathcal{D}}}{\langle\mathcal{F}\rangle_{\mathcal{D}}}\mathcal{I}^{(2)}_{\mathcal{D}}(\mathcal{F}) + \left(1 - \frac{\langle\mathcal{N}\rangle_{\mathcal{D}}}{\langle\mathcal{F}\rangle_{\mathcal{D}}}\right)\mathcal{I}^{(0)}_{\mathcal{D}}(\mathcal{F})\,\Lambda^{(2)}$$

where $\Lambda^{(2)}$ is a 2^{nd} rank tensor (i.e. a matrix). Substitution in (25) yields

$$\widehat{\sigma}_{\mathcal{D}}(f) = \widehat{\sigma}_{\mathcal{D}}(\mathcal{F}) - \Lambda^{(2)} \tag{25}$$

where

$$\begin{aligned}\Lambda^{(2)} &= \frac{\langle\mathcal{F}\rangle_{\mathcal{D}}}{\langle\mathcal{F}\rangle_{\mathcal{D}} - \langle\mathcal{N}\rangle_{\mathcal{D}}}\frac{\mathcal{I}^{(2)}_{\mathcal{D}}(\mathcal{N}) - \frac{\langle\mathcal{N}\rangle_{\mathcal{D}}}{\langle\mathcal{F}\rangle_{\mathcal{D}}}\mathcal{I}^{(2)}_{\mathcal{D}}(\mathcal{F})}{\mathcal{I}^{(0)}_{\mathcal{D}}(\mathcal{F})} \\ &= \frac{1}{\langle\mathcal{F}\rangle_{\mathcal{D}} - \langle\mathcal{N}\rangle_{\mathcal{D}}}\frac{\langle\mathcal{F}\rangle_{\mathcal{D}}\mathcal{I}^{(2)}_{\mathcal{D}}(\mathcal{N}) - \langle\mathcal{N}\rangle_{\mathcal{D}}\mathcal{I}^{(2)}_{\mathcal{D}}(\mathcal{F})}{\mathcal{I}^{(0)}_{\mathcal{D}}(\mathcal{F})}\end{aligned}$$

IV. ACCURACY.

In this section the accuracy achievable by the algorithms described above will be assessed by applying the procedures to synthetic images for the two cases of homogeneous (IV A) and inhomogeneous (IV B) noise. All synthetic images were produced with Mathematica[2] and processed with a tool developped in *C* language exploiting the freely available image processing library GraphicsMagick[3].

A. Homogeneous noise.

In order to assess the accuracy of the procedure, several hundreds synthetic images have been created by adding a signal to an image with a known noise content. The intensity distribution (extracted from a typical background image) is plotted in fig. (10a) and was used to generate 8 and 12 bit (see fig. (10b)) synthetic images free from artifacts. Composite assembly in fig. (11) contains the thumbnails relative to a sequence of images obtained from (26) for $\sigma_{xx} = 100, 200, \ldots, 800$ and $\mathcal{N} = 0.1$ (10% of full scale value). Both the ellipses drawn around the signal spot tag the ROIs obtained through the algorithm (1), the smaller being the result of applying the (optional) noise reduction procedure (line 2).

$$S = \mathcal{N}\cdot\exp\left[-\frac{1}{2}(w - w_0)^{\mathrm{T}}\cdot\widehat{\Sigma}^{-1}\cdot(w - w_0)^{\mathrm{T}}\right] \tag{26}$$

where

$$w_0 = \begin{pmatrix} 250 \\ 350 \end{pmatrix} \qquad \Sigma = \begin{pmatrix} \sigma_{xx} & \frac{\sigma_{xx}}{3} \\ \frac{\sigma_{xx}}{3} & \frac{\sigma_{xx}}{2} \end{pmatrix} \tag{27}$$

Composite assembly in fig. (11) contains the thumbnails relative to a sequence of images obtained from (26) for $\sigma_{xx} = 100, 200, \ldots, 900$ and $\mathcal{N} = 0.1$ (10% of full scale value). Both the ellipses drawn around the signal spot tag the ROIs obtained through the algorithm (1), the smaller being the result of applying the (optional) noise reduction procedure (line 2).
In fig. (12) the reconstructed σ_{xx} for a gaussian signal as described by eq. (26,27) is plotted vs the value of n used to define the ROI (domain $\mathcal{D}$ in formula (16)).Two remarks are in order at this point:

i) a higher graylevel depth **do not** provide substantially more accurate results;

ii) accuracy on components of σ are instead strongly correlated to a correct assessment of the noise level (variable κ in formula (11)), as is shown in figs. (13a) and (13b) where relative error on κ is plotted along with relative error on σ_{xx}. Note also that for too small values of n the reconstructed values suffer a strong bias from the tails of the signal still present in the corona of the ROI used to measure κ.

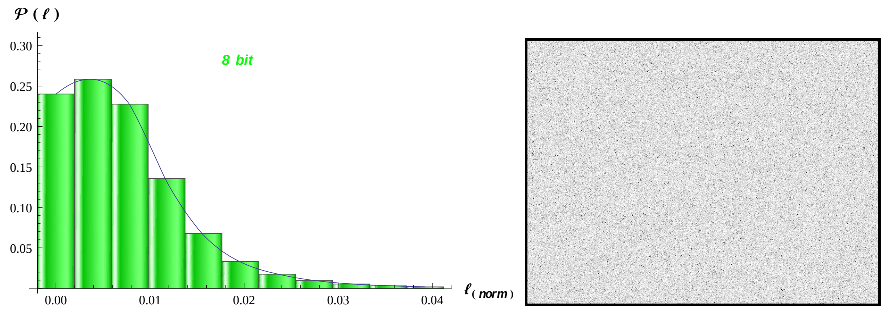

(a) (b)

Figure 10: **(a)** Typical intensity distribution extracted from a synthetic background images; ℓ is the normalized intensity (i.e. $\ell = 0, 1$ corresponds to full black/white);
(b) the 12-bit image generated according to distribution in (10a). The image has been normalized and negated to improve clarity.

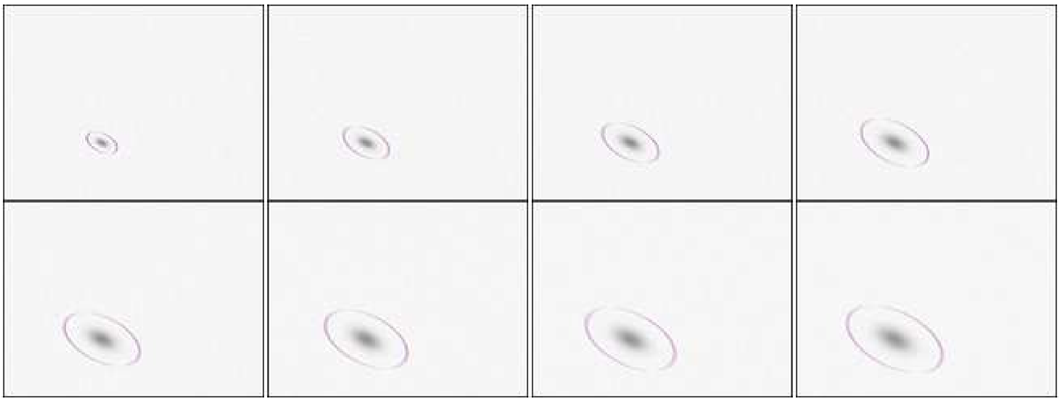

Figure 11: Syntethic gaussian signals added to background image in fig. (10b). Matrix Σ aspect ratio is as specified in eq. (27) with $\sigma_{xx} = 100, 200, \ldots, 800$ (left to right, top to bottom) and $\mathcal{N}$ =0.1. The red/blue ellipses tag the $n = 6$ ROIs for 8 and 12 bit images, respectively. An unusually high value has been chosen for n only to make the two cases more easily discernible.

The ellipses surrounding the signal in the thumbnails in fig. (14) identify the $n = 4$ contours associated to ROI's and reconstructed $\widehat{\sigma}$'s for a gaussian signal of aspect ratio as specified in eq. (27) and $\sigma_{xx} = 900$. The Signal(peak)-to-Noise(average) ratio is (from left to right, top to bottom) $\mathcal{S}/\mathcal{N} = \{1.36, 2.72, 5.43, 10.9, 21.7, 43.5, 87.0\}$. The red/blue ellipses identify the $n = 4$ contours for ROI's and reconstructed $\widehat{\sigma}$, respectively. Note that ROI's tagging works even in the more unfavourable case where noise level - although lower on average - can be higher than signal because of fluctuations. In fig (15) is plotted the behaviour of relative error on σ_{xx} vs Signal(peak)-to-Noise(average) ratio for the case described in fig. (14) and $\sigma_{\mathrm{xx}} = 300$. Consider, to this purpose, the x and y projections of the synthetic image in the top-left corner of fig. (14)

B. Inhomogeneous noise.

In all the cases that (11) cannot be applied, the more general approach based on eqs. (10) must be followed. Although - as before - one is not interested in the detailed topological properties of the noise, nevertheless its structure affects momenta $\mathcal{I}_{\mathcal{D}}^{(k)}[n]$. The only reasonable procedure, therefore, seems that of directly extracting those quantities from the the area corresponding to the same ROI in background images and exploiting linearity (that is, eqs. (10)). In order to assess the performances of this approach, a large number of 16−bit synthetic images has been created aiming at mimicking the conditions met during real experiments. The image format

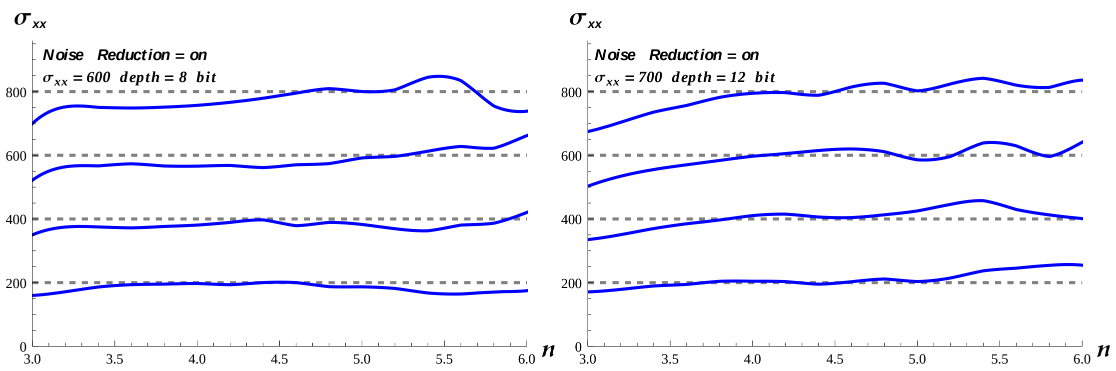

(a) (b)

Figure 12: Reconstructed σ_{xx} vs n for a gaussian signal as described by eqs. (26) and (27) for 8 **(a)** and 12 **(b)** bit images. Black, dashed lines are the exact value used to generate the synthetic images.

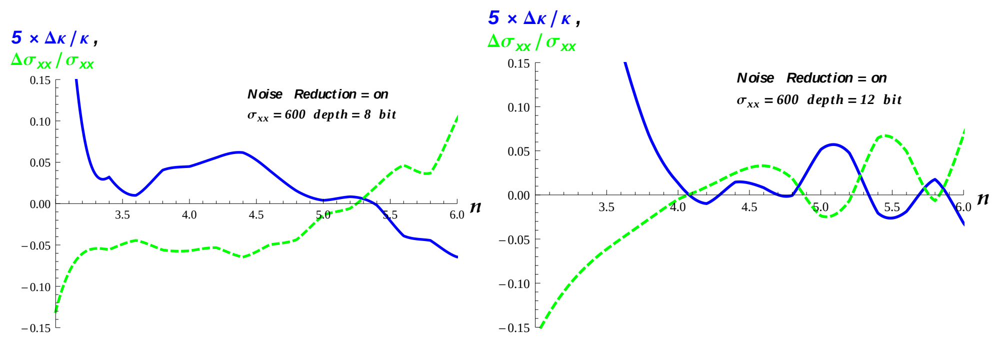

(a) (b)

Figure 13: Relative error on κ (solid, blue) and σ_{xx} (dashed, green) for $\sigma_{\rm xx} = 700$. Note: $\Delta\kappa/\kappa$ has been multiplied by 5 to clarify the strong correlation with $\Delta\sigma_{\rm xx}/\sigma_{\rm xx}$.

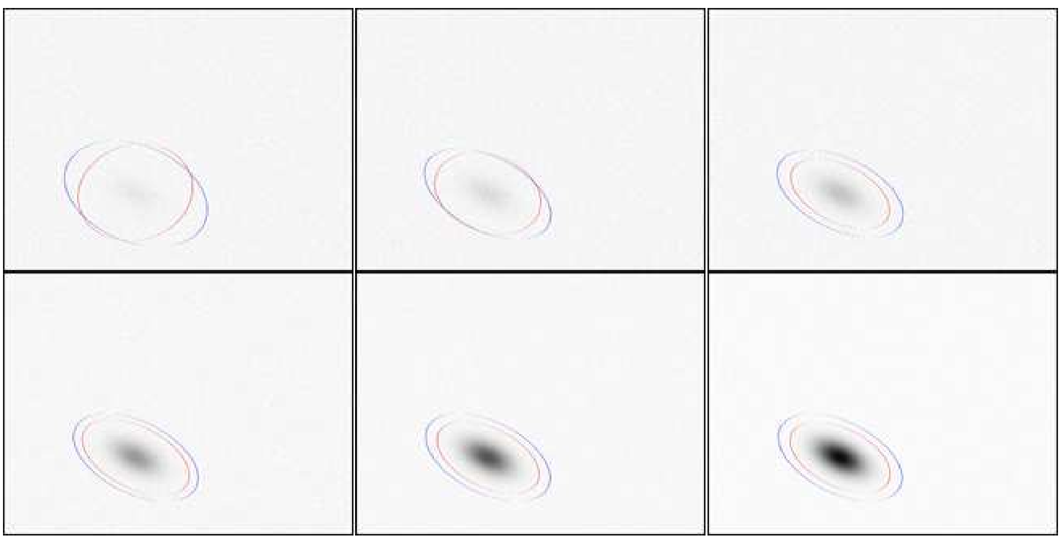

Figure 14: Syntethic images obtained by adding to background image in fig. (10b) a gaussian signals with fixed aspect ratio and size. The red/blue ellipses identify the $n = 4$ contours for ROI's and reconstructed $\widehat{\sigma}$, respectively.

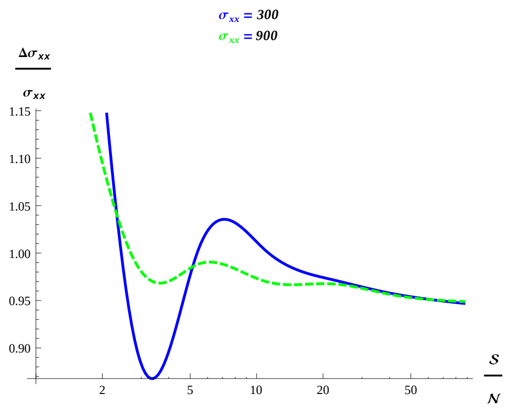

Figure 15: Relative error σ_{xx} vs Signal(peak)-to-Noise(average) ratio for $\sigma_{xx} = 300$ (solid, blue) and $\sigma_{xx} = 900$ (dashed, green). The accuracy is fairly good also for the more unfavourable cases.

reflect the operation conditions of SPARC experiment as of fall 2010, namely 16−bit with 12−bit quantization, and where built superimposing

- an impulsive (a.k.a. "salt-and-pepper" or "shot") noise, with only two possible outcomes, $2^{\mathrm{n_{bit}}} - 1$ ($n_{\mathrm{bit}} = 12$) and 0, with probability μ_{SN};
- a poissonian noise with normalized average μ_{PN};
- a gaussian signal and background

$$\mathcal{F}_{\mathcal{X}}\left(w\right) = \mathcal{A}_{\mathcal{X}} \exp\left[-\frac{1}{2}\left(w - w_{\mathcal{X}}\right)^{\mathrm{T}} \cdot \Sigma_{\mathcal{X}}^{-1} \cdot \left(w - w_{\mathcal{X}}\right)\right] \qquad \mathcal{X} = \mathcal{S}, \mathcal{B} \tag{28}$$

of center and r.m.s. matrix

$$w_{\mathcal{S}} = \begin{pmatrix} 200 \\ 350 \end{pmatrix} \qquad \Sigma_{\mathcal{S}} = \begin{pmatrix} 12 \cdot 10^2 & 8 \cdot 10^2 \\ 8 \cdot 10^2 & 24 \cdot 10^2 \end{pmatrix} \tag{29}$$

and

$$w_{\mathcal{B}} = \begin{pmatrix} 300 \\ 250 \end{pmatrix} \qquad \Sigma_{\mathcal{B}} = \begin{pmatrix} 24 \cdot 10^4 & -8 \cdot 10^4 \\ -8 \cdot 10^4 & 12 \cdot 10^4 \end{pmatrix} \tag{30}$$

respectively. For the background the amplitude has been kept fixed to $A_{\mathcal{B}} = 0.01$. For the signal the values $A_{\mathcal{S}} = 0.02, 0.04, 0.08$ have been considered. Since the signal is normalized to $\mathcal{N}_{\mathcal{X}} = 2\pi\mathcal{A}_{\mathcal{X}}\sqrt{\det \Sigma_{\mathcal{X}}}$, the values chosen correspond to signal-to-noise ratio of $\frac{\mathcal{N}_{\mathcal{S}}}{\mathcal{N}_{\mathcal{B}}} = 0.2, 0.4\,\mathrm{and}\,0.8$, respectively. Common values for laser driven-to-dark current total charge ratio at SPARC fluctuate around 0.4.

The values considered for μ_{SN} are $\{1, 2, 4, 10, 20, 40\} \cdot 10^{-3}$. The values considered for μ_{PN} are $\{1, 5, 10, 15\} \cdot 10^{-3}$, normalized to 8−bit images full scale (i.e. the corresponding average gray levels used to generate Poisson random variates equal $0.256, 1.28, 2.56, 3.84$, respectively). The distributions obtained have been interpolated and adapted to generate 16−bit deviates. This induces a negligible distortion in the actual average value of deviates, except for the case $\mu_{\mathrm{PN}} = 1{\cdot}10^{-3}$, for which the effective normalized noise level coresond to $2.4{\cdot}10^{-3}$. The values considered for μ_{PN}, $A_{\mathcal{S}}$ and $A_{\mathcal{B}}$ reflect the requirement of producing 16−bit images with 12−bit quantization, so that maximum gray level does not exceed $2^{\mathrm{n_{bit}}} - 1$ (mimicking a higher resolution than that actually available). An example of the synthetic images is shown in fig. (16), while the reconstructed r.m.s matrix as a function of n is shown in fig. (17) for several different values of signal ($\mathcal{A}_{\mathcal{S}}$) and noise ($\mu_{\mathrm{PN}}, \mu_{\mathrm{SN}}$) amplitudes.

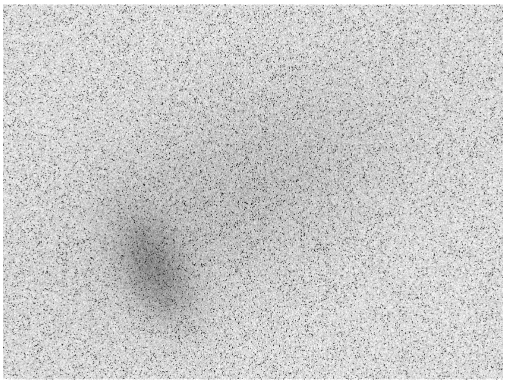

Figure 16: A synthetic image featuring a gaussian spot superimposed to a combiantion of both impulsive and poissonian noise, plus a wide gaussian background. The following set of parameters was used $A_{\mathcal{S}} = 0.020, A_{\mathcal{B}} = 0.010, \mu_{\mathrm{PN}} = 0.015, \mu_{\mathrm{SN}} = 0.040$. Gaussian background (formulæ(28-30) is scarcely visible because of low contrast. For the case shown the ratio between signal and background normalization is $\mathcal{N}_{\mathcal{S}}/\mathcal{N}_{\mathcal{B}} = 0.2$.

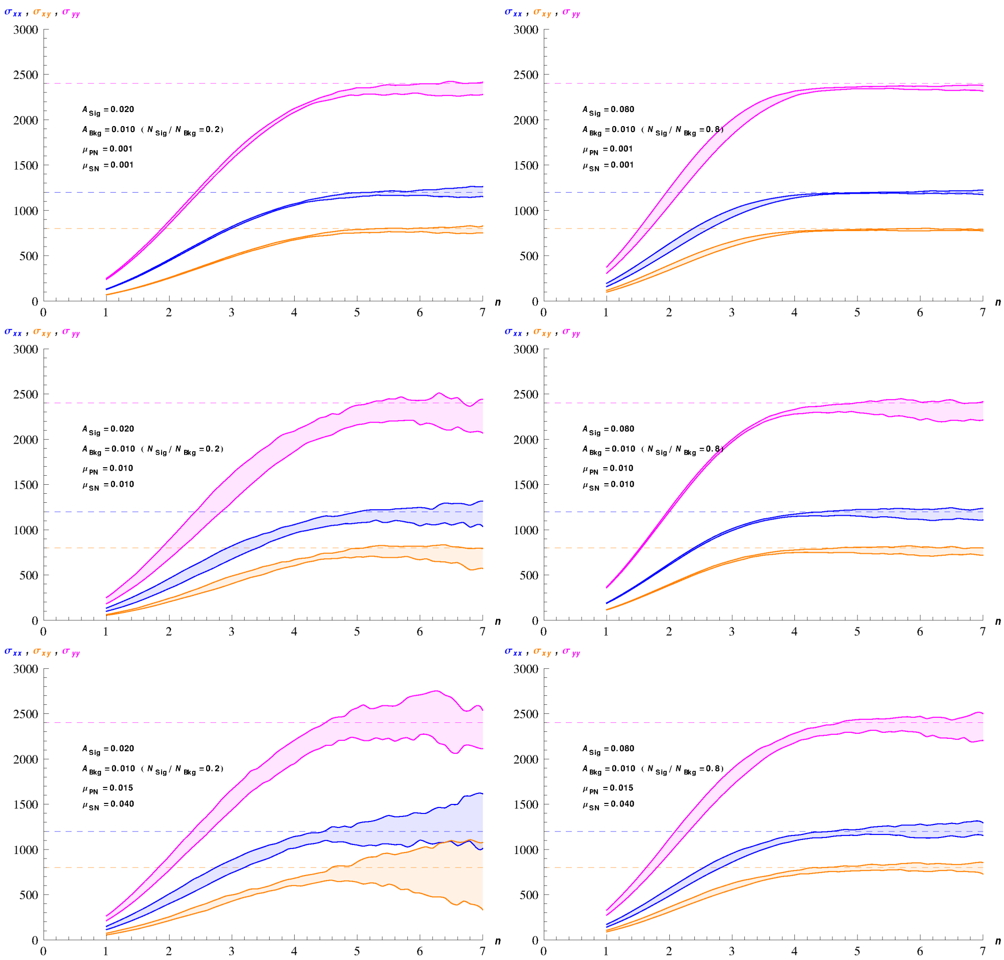

Figure 17: Reconstructed σ_{xx}, σ_{xy} and σ_{yy} vs n for the gaussian signal described by eq. (28) superimposed to a wider, off-center gaussian background affected by impulsive and poissonian noise (see eqs. (28-29)). Dashed lines correspond to exact values used to generate the synthetic images. Coloured bands define the $\pm 1\sigma$ region (computed over a sample of 200 images) around the reconstructed value.

In figs. (17) are shown the reconstructed σ's for increasing $\mathcal{A}_\mathcal{S}/\mathcal{A}_\mathcal{B}$ ratio (left to right) and increasing level of both poissonian and impulsive noise (top to bottom) as a function of n. It is clearly visible the effect of increasing noise on the statistical fluctuations, signaled by the width of coloured bands, which delimit the $\pm 1\sigma$ region around the reconstructed value.

V. IMAGE GALLERY. LASER SPOT. HIGH ASPECT RATIO.

In fig. (18) is shown the outcome of the procedure applied to an image of the laser beam used to drive bunch emission from SPARC RF-gun photocathode. The offset subtraction described in Algorithm (1), line (3), which is irrelevant for ROI identification (for the algorithm exploits the effective level range in the image, line (7)), proves instead essential for this 12−bit image (although the format is 16−bit indeed) affected by a tiny dynamical range of the signal compared to the very large average background (due presumably to LabView's convention for image data storage). To images affected by this problem applies the remark at the end of sec. (IV), for in these cases the ratio between average noise level and total is very close to its upper bound $\kappa / \langle F \rangle_\mathcal{D} \leq 1$.

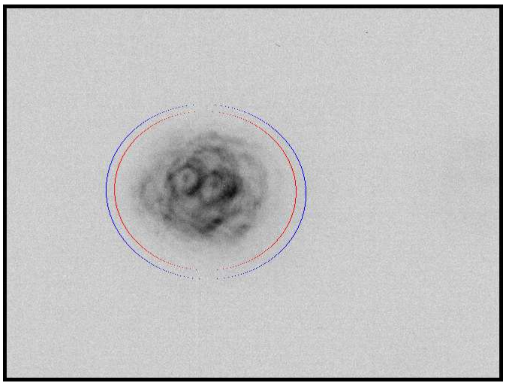

Figure 18: Spot of the laser beam used to extract electrons from the SPARC RF-gun photocathode. The red/blue ellipses identify the $n = 3$ contours for ROI's and reconstructed r.m.s. $\widehat{\sigma}$, respectively.

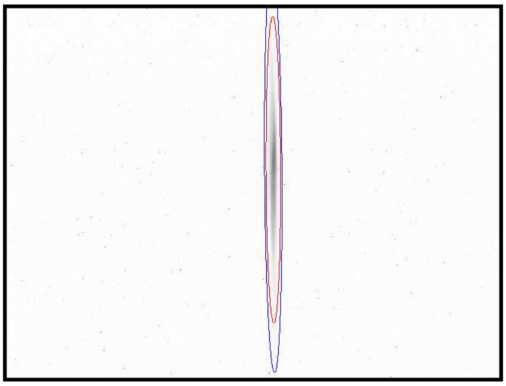

Figure 19: An electron beam spot (12-bit) image acquired during a 4-pole scan. As in previous images, red/blue ellipses tag the $n = 4$ contours associated to ROI's and reconstructed $\widehat{\sigma}$, respectively.

Fig. (19) shows the spot produced onto the Cromox target by the by the electron beam during a 4-pole scan for emittance measurement. The algorithm adapts nicely also to images affected by a remarkably high aspect ratio.

VI. CONCLUSIONS

In this note two algorithms have been discussed aimimg at

i) identifying the Region Of Interest the signal presumably reside upon. The algorithm does not need any background image to be acquired, adapts well in a wide range of cases like imaging of laser, electron beams of different aspect ratios and sizes. Analysis of performances suggests that the core algorithm can reliably identify a ROI on an image-by-image base in few tenths of milliseconds, to which must be summed the overheads due e.g. to memory and/or storage; given these results, a real time implementation is more than a chance;

ii) measuring statistical properties of the signal (2D r.m.s. matrix, centroid) essential for a varieties of purposes (fine tuning of laser spot size and alignment, emittance measurement etc.); the approach avoids the cumbersome task of a detailed disentanglement of the signal from noise, making only a reasonable (yet unproved) assumption about the topological properties of the background.

In a forthcoming note the practical implementation of the algorithm described above in the framework of SPARC control and acquisition system will be addressed, along with the possibility of obtaining substantial speed-ups through the deployment of the code on massively parallel, multi-core GPUs[4].

.

[1] SPARC Collaboration. Homepage http://www.sparc.it.
[2] Wolfram Research Inc. Homepage http://www.wolfram.com/mathematica.
[3] GraphicsMagick Group. Homepage http://www.graphicsmagick.org.
[4] NVIDIA Corporation. Homepage http://www.nvidia.com/object/cuda_home_new.html.

Appendices

A. TRANSFORMATIONS IN THE PLANE: VECTORS

Let (ξ, η) be the rotated coordinate system where the ROI (see fig.(8)) turns to be an *upright* ellipse. The associated versors $\widehat{u}_\xi, \widehat{u}_\eta$ can be expressed in terms of the versors $\widehat{u}_x, \widehat{u}_y$ associated to the camera frame in terms of a 2D rotation matrix:

$$\begin{pmatrix} \widehat{u}_\xi \\ \widehat{u}_\eta \end{pmatrix} = \widehat{R}\,(\phi) \cdot \begin{pmatrix} \widehat{u}_x \\ \widehat{u}_y \end{pmatrix} \tag{A1}$$

where

$$\widehat{R}\,(\phi) = \begin{pmatrix} \cos\phi & \sin\phi \\ -\sin\phi & \cos\phi \end{pmatrix}, \qquad \widehat{R}^{-1}\,(\phi) = \widehat{R}^{\mathrm{T}}\,(\phi) = \widehat{R}\,(-\phi) \tag{A2}$$

The vector associated to a given point on the plane can be expressed indifferently as

$$\overrightarrow{v} = x \cdot \widehat{u}_x + y \cdot \widehat{u}_y = \overrightarrow{\delta} + \xi \cdot \widehat{u}_\xi + \eta \cdot \widehat{u}_\eta$$

that is

$$\overrightarrow{v} = \begin{pmatrix} x & , & y \end{pmatrix} \cdot \begin{pmatrix} \widehat{u}_x \\ \widehat{u}_y \end{pmatrix} = \begin{pmatrix} d_x & , & d_y \end{pmatrix} \cdot \begin{pmatrix} \widehat{u}_x \\ \widehat{u}_y \end{pmatrix} + \begin{pmatrix} \xi & , & \eta \end{pmatrix} \cdot \widehat{R}\,(\phi) \cdot \begin{pmatrix} \widehat{u}_x \\ \widehat{u}_y \end{pmatrix}$$

It is readily shown that

$$
\begin{aligned}
\begin{pmatrix} x \\ \\ y \end{pmatrix} &= \widehat{R}^{\mathrm{T}}(\phi)\cdot\begin{pmatrix} \xi \\ \\ \eta \end{pmatrix}+\begin{pmatrix} d_x \\ \\ d_y \end{pmatrix} \\
\begin{pmatrix} \xi \\ \\ \eta \end{pmatrix} &= \widehat{R}(\phi)\cdot\begin{pmatrix} x-d_x \\ \\ y-d_y \end{pmatrix}
\end{aligned}
\tag{A3}
$$

B. TRANSFORMATIONS IN THE PLANE: TENSORS

From eqs (7),(8) and (A3) follows that

$$
w=\widehat{R}^{\mathrm{T}}(\phi)\,\omega+d
$$

implying that

$$
d^2w=\left|\frac{\partial w}{\partial\omega}\right|d^2\omega=\left|\det\widehat{R}^{\mathrm{T}}(\phi)\right|d^2\omega=d^2\omega
$$

Moreover, domain (6) can be expressed in rotated coordinates as

$$
\begin{aligned}
\mathcal{D}=\Delta \;&\equiv\; \left\{\omega\ni\omega^{\mathrm{T}}\cdot\widehat{R}(\phi)\,\widehat{\mathcal{S}}^{-1}\cdot\widehat{R}^{\mathrm{T}}(\phi)\,\omega\le n^2\right\} \\
&= \left\{\omega\ni\omega^{\mathrm{T}}\cdot\widehat{\Sigma}^{-1}\cdot\omega\le n^2\right\}
\end{aligned}
\tag{B4}
$$

where

$$
\widehat{\Sigma}^{-1}\equiv\widehat{R}(\phi)\,\widehat{\mathcal{S}}^{-1}\cdot\widehat{R}^{\mathrm{T}}(\phi)\Longleftrightarrow\widehat{\Sigma}\equiv\widehat{R}^{\mathrm{T}}(\phi)\,\widehat{\mathcal{S}}\cdot\widehat{R}(\phi)
$$

so that (B4) reads

$$
\Delta=\mathcal{D}\equiv\left\{\omega\ni\omega^{\mathrm{T}}\cdot\widehat{\Sigma}^{-1}\cdot\omega\le n^2\right\}
\tag{B5}
$$

Since by construction $\widehat{\Sigma}(\Phi)$ is diagonal

$$
\widehat{\Sigma}=\begin{pmatrix}\Sigma_{\xi\xi} & 0 \\ \\ 0 & \Sigma_{\eta\eta}\end{pmatrix}\Longrightarrow\widehat{\Sigma}^{-1}=\begin{pmatrix}\dfrac{1}{\Sigma_{\xi\xi}} & 0 \\ 0 & \dfrac{1}{\Sigma_{\eta\eta}}\end{pmatrix}
$$

then

$$
\Delta=\mathcal{D}\equiv\left\{(\xi,\eta)\ni\frac{\xi^2}{\Sigma_{\xi\xi}}+\frac{\eta^2}{\Sigma_{\eta\eta}}\le n^2\right\}
\tag{B6}
$$

Note that the area of the the domain Δ is

$$
\mathcal{A}_{\mathcal{D}}=\mathcal{A}_{\Delta}=\pi n^2\sqrt{\Sigma_{\xi\xi}\Sigma_{\eta\eta}}=\pi n^2\sqrt{\det\widehat{\Sigma}}=\pi n^2\sqrt{\det\widehat{\mathcal{S}}}
\tag{B7}
$$

Note also that d is the position vector of the point of coordinates $(\xi,\eta)=(0,0)$ in the rotated frame:

$$
\begin{aligned}
\mathcal{I}^{(2)}_{\mathcal{D}}(F) \;&=\; \int_\Delta d^2\omega\,\mathcal{F}\left(\widehat{R}^{\mathrm{T}}(\phi)\,\omega+d\right)\left\{\left[\widehat{R}^{\mathrm{T}}(\phi)\,\omega+d\right]\cdot\left[\omega^{\mathrm{T}}\widehat{R}(\phi)+d^{\mathrm{T}}\right]\right\} \\
&= \int_\Delta d^2\omega\,\Phi(\omega)\left[\widehat{R}^{\mathrm{T}}(\phi)\left(\omega\cdot\omega^{\mathrm{T}}\right)\widehat{R}(\phi)+\left[d\cdot d^{\mathrm{T}}\right]+\widehat{R}^{\mathrm{T}}(\phi)\left(\omega\cdot d^{\mathrm{T}}\right)+\left(d\cdot\omega^{\mathrm{T}}\right)\widehat{R}(\phi)\right] \\
&= \widehat{R}^{\mathrm{T}}(\phi)\left\{\int_\Delta d^2\omega\,\Phi(\omega)\left[\omega\cdot\omega^{\mathrm{T}}\right]\right\}\widehat{R}(\phi)+\left[d\cdot d^{\mathrm{T}}\right]\left\{\int_\Delta d^2\omega\,\Phi(\omega)\right\} \\
&\quad +\widehat{R}^{\mathrm{T}}(\phi)\left\{\int_\Delta d^2\omega\,\Phi(\omega)\,\omega\right\}d^{\mathrm{T}}+d\cdot\left\{\int_\Delta d^2\omega\,\Phi(\omega)\,\omega^{\mathrm{T}}\right\}\widehat{R}(\phi)
\end{aligned}
\tag{B8}
$$

where

$$\Phi(\omega) \equiv \mathcal{F}\left[\widehat{R}^{\mathrm{T}}(\phi)\,\omega + d\right]$$

Result (B8) may be cast in the more suggestive form

$$\mathcal{I}_{\mathcal{D}}^{(2)}(\mathcal{F}) = \widehat{R}^{\mathrm{T}}(\phi)\,\mathcal{I}_{\Delta}^{(2)}(\Phi)\,\widehat{R}(\phi) + \left[d \cdot d^{\mathrm{T}}\right]\mathcal{I}_{\Delta}^{(0)}(\Phi) + \widehat{R}^{\mathrm{T}}(\phi)\,\mathcal{I}_{\Delta}^{(1)}(\Phi) \cdot d^{\mathrm{T}} + d \cdot \mathcal{I}_{\Delta}^{(1)\mathrm{T}}(\Phi)\,\widehat{R}(\phi)$$

where symbol $\mathcal{I}_{\Delta}^{(\mathrm{n})}$ is a n^{th}-rank tensor representing the components of distribution's momentum of the same order **with respect to rotated axes**. Derivation of $\overrightarrow{d}$'s components in the rotated frame

$$\delta = \begin{pmatrix} \delta_\xi \\ \\ \delta_\eta \end{pmatrix} \equiv \begin{pmatrix} \overrightarrow{d} \cdot \widehat{u}_\xi \\ \\ \overrightarrow{d} \cdot \widehat{u}_\eta \end{pmatrix} = \widehat{R}(\phi) \begin{pmatrix} (d_{\mathrm{x}}\widehat{u}_{\mathrm{x}} + d_{\mathrm{y}}\widehat{u}_{\mathrm{y}}) \cdot \widehat{u}_{\mathrm{x}} \\ \\ (d_{\mathrm{x}}\widehat{u}_{\mathrm{x}} + d_{\mathrm{y}}\widehat{u}_{\mathrm{y}}) \cdot \widehat{u}_{\mathrm{y}} \end{pmatrix} = \widehat{R}(\phi) \begin{pmatrix} d_{\mathrm{x}} \\ \\ \mathrm{d}_{\mathrm{y}} \end{pmatrix} = \widehat{R}(\phi) \cdot d$$

provide a way to recast $\mathcal{I}_{\mathcal{D}}^{(2)}(F)$ in the more compact form

$$\mathcal{I}_{\mathcal{D}}^{(2)}(\mathcal{F}) = \widehat{R}^{\mathrm{T}}(\phi)\left[\mathcal{I}_{\Delta}^{(2)}(\Phi) + \left(\delta \cdot \delta^{\mathrm{T}}\right)\mathcal{I}_{\Delta}^{(0)}(\Phi) + \mathcal{I}_{\Delta}^{(1)}(\Phi) \cdot \delta^{\mathrm{T}} + \delta \cdot \mathcal{I}_{\Delta}^{(1)\mathrm{T}}(\Phi)\right]\widehat{R}(\phi) \tag{B9}$$

Much in the same way it is easily proven that

$$\mathcal{I}_{\mathcal{D}}^{(0)}(\mathcal{F}) = \mathcal{I}_{\Delta}^{(0)}(\Phi) \tag{B10}$$

(conservation of distribution integral) and that

$$\mathcal{I}_{\mathcal{D}}^{(1)}(\mathcal{F}) = \widehat{R}^{\mathrm{T}}(\phi)\left[\mathcal{I}_{\Delta}^{(1)}(\Phi) + \mathcal{I}_{\Delta}^{(0)}\delta\right] \tag{B11}$$

In the case that the ROI's center and the function's barycentre coincide (i.e. $\mathcal{I}_{\Delta}^{(1)}(\Phi) = 0$) the (B9) is nothing but the Huygens-Steiner theorem (connecting the moment of inertia of a rigid body about any axis, given the moment of inertia of the object about the parallel axis through the object's centre of mass).

Moreover, eqs. (B9,B10,B11) establish the expected result that covariance tensors $\widehat{\sigma}_\Delta(\Phi)$ and $\widehat{\sigma}_{\mathcal{D}}(F)$ transform consistently under the change of coordinates $(\xi, \eta) \to (x, y)$:

$$\begin{aligned}
\widehat{\sigma}_{\mathcal{D}}(\mathcal{F}) &\equiv \frac{\mathcal{I}_{\mathcal{D}}^{(2)}(\mathcal{F})}{\mathcal{I}_{\mathcal{D}}^{(0)}(\mathcal{F})} - \frac{\mathcal{I}_{\mathcal{D}}^{(1)}(\mathcal{F}) \cdot \mathcal{I}_{\mathcal{D}}^{(1)\mathrm{T}}(\mathcal{F})}{\left[\mathcal{I}_{\mathcal{D}}^{(0)}(\mathcal{F})\right]^2} \\
&= \widehat{R}^{\mathrm{T}}(\phi)\left\{\frac{\mathcal{I}_{\Delta}^{(2)}(\Phi) + \left(\delta \cdot \delta^{\mathrm{T}}\right)\mathcal{I}_{\Delta}^{(0)}(\Phi) + \mathcal{I}_{\Delta}^{(1)}(\Phi) \cdot \delta^{\mathrm{T}} + \delta \cdot \mathcal{I}_{\Delta}^{(1)\mathrm{T}}(\Phi)}{\mathcal{I}_{\Delta}^{(0)}(\Phi)}\right. \\
&\qquad\qquad \left. - \frac{\left[\mathcal{I}_{\Delta}^{(1)}(\Phi) + \mathcal{I}_{\Delta}^{(0)}\delta\right] \cdot \left[\mathcal{I}_{\Delta}^{(1)}(\Phi) + \mathcal{I}_{\Delta}^{(0)}\delta\right]^{\mathrm{T}}}{\left[\mathcal{I}_{\Delta}^{(0)}(\Phi)\right]^2}\right\}\widehat{R}(\phi) \\
&= \widehat{R}^{\mathrm{T}}(\phi)\left\{\frac{\mathcal{I}_{\Delta}^{(2)}(\Phi)}{\mathcal{I}_{\Delta}^{(0)}(\Phi)} - \frac{\mathcal{I}_{\Delta}^{(1)}(\Phi) \cdot \mathcal{I}_{\Delta}^{(1)\mathrm{T}}(\Phi)}{\left[\mathcal{I}_{\Delta}^{(0)}(\Phi)\right]^2}\right\}\widehat{R}(\phi)
\end{aligned}$$

that is

$$\widehat{\sigma}_{\mathcal{D}}(\mathcal{F}) = \widehat{R}^{\mathrm{T}}(\phi)\,\widehat{\sigma}_\Delta(\Phi)\,\widehat{R}(\phi) \tag{B12}$$

Let us now compute

$$\mathcal{J}_{\mathcal{D}}^{(2)} \equiv \int_{\mathcal{D}} d^2w\ \left(w \cdot w^{\mathrm{T}}\right) \tag{B13}$$

by exploiting eqs. (A1),(B6).

$$\begin{aligned}
\mathcal{J}_{\mathcal{D}}^{(2)} &= \int_{\mathcal{D}} dw\left[w \cdot w^{\mathrm{T}}\right] \\
&= \int_{\Delta} d\omega\left[\left(\widehat{R}^{\mathrm{T}}(\phi)\,\omega + d\right) \cdot \left(\omega^{\mathrm{T}}\widehat{R}(\phi) + d^{\mathrm{T}}\right)\right] \\
&= \widehat{R}^{\mathrm{T}}(\phi)\left[\int_{\Delta} d\omega\left(\omega \cdot \omega^{\mathrm{T}}\right)\right]\widehat{R}(\phi) + \left[d \cdot d^{\mathrm{T}}\right]\mathcal{A}_{\Delta}
\end{aligned}$$

From (B6) it follows that

$$\int_{\Delta} d^2\omega\left(\omega \cdot \omega^{\mathrm{T}}\right) = \int_{-a}^{+a} d\xi \int_{-b\sqrt{1-\left(\frac{\xi}{a}\right)^2}}^{+b\sqrt{1-\left(\frac{\xi}{a}\right)^2}} d\eta \begin{pmatrix} \xi^2 & \xi\eta \\ \eta\xi & \eta^2 \end{pmatrix}$$

where

$$\begin{aligned}
a &\equiv n\sqrt{\Sigma_{\xi\xi}} \\
b &\equiv n\sqrt{\Sigma_{\eta\eta}}
\end{aligned}$$

which implies

$$\int_{\Delta} d^2\omega\left(\omega \cdot \omega^{\mathrm{T}}\right) = \frac{1}{4}\pi ab \begin{pmatrix} a^2 & 0 \\ 0 & b^2 \end{pmatrix} = \frac{n^2}{4}\mathcal{A}_{\Delta} \begin{pmatrix} \Sigma_{\xi\xi} & 0 \\ 0 & \Sigma_{\eta\eta} \end{pmatrix} = \frac{n^2}{4}\mathcal{A}_{\Delta}\widehat{\Sigma} \tag{B14}$$

that is

$$\mathcal{J}_{\mathcal{D}}^{(2)} = \mathcal{A}_{\Delta}\left\{\frac{n^2}{4}\overbrace{\left[\widehat{R}^{\mathrm{T}}(\phi) \cdot \widehat{\Sigma} \cdot \widehat{R}(\phi)\right]}^{\widehat{\mathcal{S}}} + d \cdot d^{\mathrm{T}}\right\} = \mathcal{A}_{\mathcal{D}}\left[\frac{n^2}{4}\widehat{\mathcal{S}} + d \cdot d^{\mathrm{T}}\right] \tag{B15}$$